PAN
ARCHIVES OF ACOUSTICS
Vol. **46**, No. 1, pp. 95–104 (2021)
DOI: 10.24425/aoa.2021.136564

Research Paper

Error Analysis of Sound Source Directivity Interpolation Based on Spherical Harmonics

Adam SZWAJCOWSKI[(1)]*, Daniel KRAUSE[(2)], Anna SNAKOWSKA[(1)]

[(1)] *Department of Robotics and Mechatronics*
AGH University of Science and Technology
Kraków, Poland
*Corresponding Author e-mail: szwajcowski@agh.edu.pl

[(2)] *Faculty of Information Technology and Communication Sciences*
Tampere University
Tampere, Finland

(*received July 16, 2020; accepted November 15, 2020*)

Precise measurement of the sound source directivity not only requires special equipment, but also is time-consuming. Alternatively, one can reduce the number of measurement points and apply spatial interpolation to retrieve a high-resolution approximation of directivity function. This paper discusses the interpolation error for different algorithms with emphasis on the one based on spherical harmonics. The analysis is performed on raw directivity data for two loudspeaker systems. The directivity was measured using sampling schemes of different densities and point distributions (equiangular and equiareal). Then, the results were interpolated and compared with these obtained on the standard 5° regular grid. The application of the spherical harmonic approximation to sparse measurement data yields a mean error of less than 1 dB with the number of measurement points being reduced by 89%. The impact of the sparse grid type on the retrieval error is also discussed. The presented results facilitate optimal sampling grid choice for low-resolution directivity measurements.

Keywords: sound source directivity; spherical harmonics; interpolation error; sparse measurements.

1. Introduction

The directivity of a sound source is one of its most important characteristics, and its determination is necessary for accurate predictions of sound wave propagation. However, analytical formulae for the sound source directivity have only been derived for simple sources such as multipoles or for sources with high levels of symmetry (e.g., a piston vibrating in an infinite baffle (Rayleigh, 1945) or the outlet of an unbaffled cylindrical wave-guide (Sinayoko *et al.*, 2010; Snakowska, Jurkiewicz, 2010)). Knowledge of the directivity enables the calculation of the field inside a duct and the radiation impedance (Snakowska *et al.*, 2017). Furthermore, shaping the sound source directivity has been the subject of research concerning reductions in environmental noise, especially aircraft noise (Joseph *et al.*, 1999). For more complex source geometries, the sound source directivity has to be derived by means of numerical or experimental methods (Duan, Kirby, 2012; Lidoine *et al.*, 2001).

Directivity measurements are commonly performed for electroacoustic sound sources such as loudspeaker systems or columns. Once the directivity has been determined, computer models of these sources can be created and later imported to acoustic simulation software. The model quality impacts the reliability of the simulation results, which is why it is important to describe these models accurately. Currently, most acoustical simulation software require input directivity data to have a resolution of 5° in both the horizontal and vertical planes, which results in a total of over 2500 measurement points (CLF, 2004; AES, 2008). Performing measurements at such a large number of points is very time-consuming, even when an automatic microphone positioning system is used.

One way of shortening the process is to measure the sound distribution over a sparse grid of points and

interpolate the results. This approach can only be used when the interpolation error is negligible for intended application. The procedure described above is common in head-related transfer function (HRTF) measurements, which involve human subjects and thus cannot last too long (Nishino *et al.*, 1999). Sound source measurements do not carry such restraints; however, long-lasting measurement processes increase the risk of changes in environmental conditions such as temperature or humidity. When there is no dedicated microphone positioning system, performing sufficiently high-resolution measurements is even more difficult. Furthermore, the final sound receiver is very often a human, whose hearing system is imperfect and insensitive to very small changes in volume. Thus, the question arises of whether it is worth trading some of the accuracy for a reduction in measurement time.

In the case of HRTFs, one of the most popular interpolation methods is to express the data in the spherical harmonic (SH) domain[1]. The first experiments utilizing this method were conducted more than 20 years ago (Evans *et al.*, 1998), but the topic is still prevalent in current research. Over the years, more specific subjects have been considered, such as extending the mathematical model to represent distance-dependent HRTFs (Zhang *et al.*, 2010), proper sampling scheme choice (Zhang *et al.*, 2012), or loudness stability when using a limited set of SH (Ben-Hur *et al.*, 2019). The main advantage of this approach comes from the continuity of the basis functions over the sphere, which translates to an infinite resolution. SH have also been used to express and analyze the directivity of various sound sources, such as loudspeaker arrays (Pasqual, 2014) or musical instruments (Shabtai *et al.*, 2017). Mobley utilized SH coefficients in the interpolation of the directivity of aircraft noise, but the interpolation was performed for changing throttle settings rather than variations in space (Mobley, 2015). Hargreaves provided a very brief analysis of the accuracy of mapping a specific sound source directivity to the SH domain (Hargreaves *et al.*, 2019).

Even though SH are commonly used to express the sound source directivity, the precision of this method, to the best of our knowledge, has not yet been thoroughly investigated. This paper aims to fill this knowledge gap by providing an in-depth analysis of error obtained when applying spherical harmonic approximation to sparse measurement data instead of performing high-resolution measurements. For this reason, two exemplary sound sources were measured on different measurement grids: equiangular (standard) and equiareal (regarded as the most efficient when transforming the data into the SH domain (Zhang *et al.*, 2012)). The obtained errors are compared with those given by alternative interpolation methods, namely the nearest neighbor, linear, and spline methods and a custom algorithm based on barycentric weights.

[1]It is important to note that expressing data in the spherical harmonic domain in most cases leads to approximation, not interpolation. See Subsec. 4.1.2 for more detailed explanation.

2. Theoretical background

Spherical harmonics are basis functions defined in the spherical coordinate system that assign a value to any pair of azimuth and inclination[2] angles ($\phi \in [0, 2\pi), \theta \in [0, \pi]$). They can be defined as both complex- and real-valued functions. A complex basis is useful for describing complex directivity, i.e., including phase information. Here, the focus is put solely on the magnitude, and thus the real basis is used. A real SH of degree l and order m is defined as:

$$Y_l^m(\phi,\theta) \equiv \begin{cases} (-1)^m \sqrt{2} C_l^m P_l^{|m|}(\cos\theta) \sin(|m|\phi), & \text{if } m < 0, \\ C_l^m P_l^m(\cos\theta), & \text{if } m = 0, \\ (-1)^m \sqrt{2} C_l^m P_l^m(\cos\theta) \cos(m\phi), & \text{if } m > 0, \end{cases} \tag{1}$$

where P_l^m is the associated Legendre function and C_l^m is the normalizing factor, defined as:

$$C_l^m \equiv \sqrt{\frac{2l+1}{4\pi} \frac{(l-|m|)!}{(l+|m|)!}}, \tag{2}$$

making the basis not only orthogonal but also orthonormal.

One can decompose any real spherical function (such as the sound source directivity) $f(\phi,\theta)$ into a set of coefficients F_{lm}, so that the following equation is satisfied:

$$f(\phi,\theta) = \sum_{l=0}^{\infty} \sum_{m=-l}^{l} F_{lm} Y_l^m. \tag{3}$$

In practical applications, the function $f(\phi,\theta)$ is not explicit and only a set of discrete values for certain directions is known. For computational purposes, the number of basis functions has to be limited. Assuming sampling in K directions $\Omega_k \equiv (\phi_k, \theta_k)$ and using all the SH up to degree and order N (later referred to as SH of maximum order N), Eq. (3) can be rearranged into the discrete form:

$$\begin{bmatrix} Y_0^0(\Omega_1) & \dots & Y_N^N(\Omega_1) \\ \vdots & \ddots & \vdots \\ Y_0^0(\Omega_K) & \dots & Y_N^N(\Omega_K) \end{bmatrix} \begin{bmatrix} F_{00} \\ \vdots \\ F_{NN} \end{bmatrix} = \begin{bmatrix} f(\Omega_1) \\ \vdots \\ f(\Omega_K) \end{bmatrix}. \tag{4}$$

[2]Vertical angle in acoustics is usually referred to as elevation angle ranging from $-\pi/2$ at the bottom to $\pi/2$ at the top; however, SH are commonly defined using inclination angle ranging from 0 at the top to π at the bottom. We decided to use the latter to avoid potential confusion caused by different SH formulae.

Solving Eq. (4) yields a set of F_{lm} coefficients, unambiguously describing the spherical function $f(\phi, \theta)$. The SH approximation of this function can be retrieved by a simple summation of the SH, with the coefficients serving as weights:

$$f_{\mathrm{SHA}}(\phi, \theta) = \sum_{l=0}^{N} \sum_{m=-l}^{l} F_{lm} Y_l^m. \tag{5}$$

3. Data preparation

3.1. Choice of exemplary sound sources

Although many commercial sound sources files are publicly available, bespoke measurements were performed for this study for two reasons. First, this approach guarantees that no smoothing or any other postprocessing has been applied. Second, it allows for the use of custom sampling schemes.

To examine the influence of individual directivity patterns on the interpolation accuracy, two exemplary sound sources were chosen. Both incorporated two-way active loudspeaker systems of similar, relatively small size (approx. $20 \times 13 \times 13$ cm). However, they had different applications: the first system (hereafter referenced as loudspeaker system A) was a professional studio monitor, whereas the second one (loudspeaker system B) was part of a low-budget stereo system. Due to their differences in quality, the directivity characteristics varied significantly (Fig. 1).

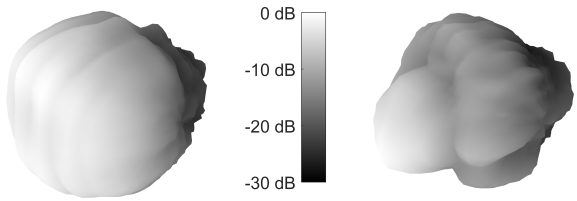

Fig. 1. Directivity balloons for the 16 kHz 1/3 octave band for loudspeaker system A (left) and loudspeaker system B (right).

3.2. Sampling schemes

3.2.1. Equiangular grid

Equiangular grids have always been the most common type for describing the directivity of electroacoustic transducers, be they sound sources or receivers. These grids comprise points lying on the crossings of equally spaced parallels and meridians. This is the current standard for the sound source directivity measurements (AES, 2008), and is commonly used in loudspeaker file formats such as GLL or CLF (CLF, 2004). An equiangular grid is both relatively simple in terms of arranging measurements and provides regularly sampled data, which are easier to process. The hierarchical structure means that coarser-resolution grids can be obtained by simple subsampling. Therefore, only one 5°-resolution measurement was performed per sound source, and then 10° and 15° data were extracted from the original measurements.

The main disadvantage of an equiangular grid is its unequal distribution of points on the sphere. While the angular difference is constant, the distance between horizontally adjacent points becomes smaller as the elevation angle increases. This results in heavy oversampling near the poles and much lower sampling density near the equator. The effective resolution is thus unequal and varies depending on the elevation angle.

3.2.2. Equiareal grid

An alternative to an equiangular grid is an equiareal grid, i.e., a grid where the sampling points are the centers of zones of equal area. This provides a more uniform representation of a spherical function, avoiding oversampling near the poles.

Equiareal or almost-equiareal grids are often used in HRTF measurements or simulations, especially in SH-related research. Recently, Lebedev's sampling scheme has become popular due to its computational advantages (Brinkmann, Weinzierl, 2018; Ben-Hur *et al.*, 2019), and some other designs have been examined to take advantage of its utility (Zhang *et al.*, 2012). None of them, however, provides perfectly equal area partitioning for an arbitrary number of sampling points, and thus another sampling scheme design algorithm was chosen.

The equiareal grid was constructed based on Leopardi's algorithm of the unit sphere partitioning (Leopardi, 2006). This algorithm was published with an associated MATLAB toolbox that allows the center points of equal area zones to be extracted (Leopardi, 2005). Using this toolbox, two grids were designed for the purpose of this research: one with 614 points and one with 266 points, corresponding to the number of sampling points in equiangular grids of 10° and 15° resolution, respectively[3] (Fig. 2).

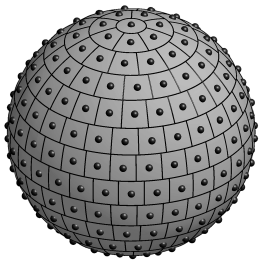

Fig. 2. Partitioning of the unit sphere into 266 equal zones using Leopardi's Recursive Zonal Equal Area Sphere Partitioning Toolbox (Leopardi, 2005).

[3]The number of points was calculated acknowledging the fact that there is only one point per pole, as at the poles the actual direction does not change with the change of the horizontal angle.

3.3. Measurement arrangement

The directivity measurements were performed in the anechoic chamber at AGH UST. The chamber is equipped with a microphone positioning system and a turntable connected to a control system that allows measurements to be automatically taken at any point on a hemisphere around the sound source (Felis *et al.*, 2012). The microphone was located 2 m away from the sound sources, which is enough to consider the directivity characteristics far-field.

As both of the measured loudspeaker systems were left–right symmetric, they were placed on their side, as shown in Fig. 3, so that the results could be mirrored to obtain the full-sphere directivity from a single hemisphere measurement. The default coordinate system was preserved, and thus the poles were located at the sides of the source, whereas usually they lie at the front and the back. This difference, however, should not substantially influence the reliability of the interpolation accuracy assessment.

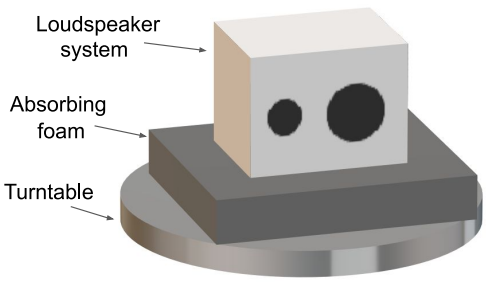

Fig. 3. Visualization of a loudspeaker system mounted on the turntable. The black circles symbolize the loudspeakers, of which the smaller one would be above the larger one when the loudspeaker system is in its normal position.

The loudspeaker systems were placed on a layer of sound-absorbing foam mounted on the turntable. The foam had the sound absorption coefficient of close to 1 starting from the 1 kHz octave band. Thus, the results for lower frequencies may have been distorted by reflections from the turntable, and were therefore excluded from the analysis. Directivity patterns for low frequencies are usually close to omnidirectional and pose less of a challenge for interpolation algorithms.

4. Computations

4.1. Spherical harmonic approximation

In this study, computations were performed using a MATLAB toolbox developed by Politis as part of his doctoral dissertation (Politis, 2016). The toolbox generates SH up to a certain maximum order and solves Eq. (4) in the least-squares sense using the following formula:

$$\mathbf{F} = \mathbf{Y}^{+}\mathbf{f}, \tag{6}$$

where $^{+}$ denotes the Moore–Penrose pseudoinverse operation and $\mathbf{F}$, $\mathbf{Y}$, and $\mathbf{f}$ denote the respective matrices from Eq. (4).

The computations were carried out using logarithmic directivity values. Since the fitting is performed in least-squares sense, it seems reasonable to minimize the errors in decibels, not in linear values, otherwise there would be large relative errors for directions of weaker sound radiation (e.g. on the back of loudspeaker systems).

4.1.1. Weights for equiangular grid

Equations (4) and (6) assume that data from all the measurement points contribute equally to determining the F_{lm} coefficients. While this is justified for equiareal grids, points on equiangular grids are not distributed evenly, and are thus associated with zones of different areas. For these grids, the data from points located near the equator should be more important than very densely arranged points near the poles. Otherwise, the resulting approximation would be well mapped near the poles, at the expense of low accuracy near the equator. This can be avoided by introducing weights to the least-squares solver. Equation (4) then takes the form:

$$(\mathbf{Y}^{\mathrm{T}}\mathbf{W}\,\mathbf{Y})\mathbf{F} = \mathbf{Y}^{\mathrm{T}}\mathbf{W}\,\mathbf{f}, \tag{7}$$

where T denotes matrix transposition and $\mathbf{W}$ is a diagonal matrix with weights for consecutive directions:

$$\mathbf{W} = \begin{bmatrix} w(\Omega_1) & 0 & \dots & 0 \\ 0 & w(\Omega_2) & & \vdots \\ \vdots & & \ddots & 0 \\ 0 & \dots & 0 & w(\Omega_K) \end{bmatrix}. \tag{8}$$

To obtain the optimal reproduction of a spherical function, the weights should be proportional to the area of the zones corresponding to each of the sampling points. The area of these zones varies along the inclination angle, and for the unit sphere the weights can be approximated as:

$$w(\Omega_k) = \Delta\phi \sin\theta_k \Delta\theta, \tag{9}$$

where $\Delta\phi$ and $\Delta\theta$ are the azimuth and inclination angle resolutions, respectively, in radians. The given formula is not appropriate for the poles ($\sin\theta_k = 0$). Instead, the weights can be approximated as the area of the circle limited by the parallel at which the inclination angle is equal to half the inclination resolution (Fig. 4):

$$w_p = \pi\left(\sin\frac{\Delta\theta}{2}\right)^2. \tag{10}$$

The given formulae for weights refer to approximated areas, assuming that the approximation error is

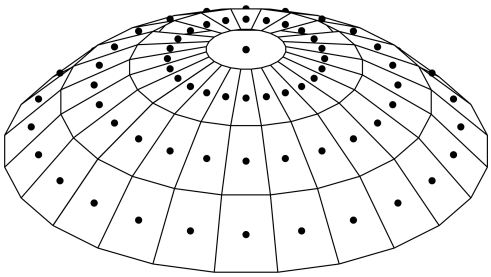

Fig. 4. Distribution of points and their respective zones near the pole on an equiangular grid of 15° resolution. The zone corresponding to the pole is approximated as a circle of the area given by Eq. (10), and the other zones are approximated as trapeziums with areas given by Eq. (9).

negligible in the field of acoustics. The exact values can be obtained by means of Neumann quadrature and are of greater interest in applications requiring much higher precision, such as in geophysics (Sneeuw, 1994).

4.1.2. Determining maximum order of spherical harmonics

In research on similar topics, the number of sampling points is usually determined based on the maximum order of SH, which is chosen according to the desired maximum spatial frequency (Zhang *et al.*, 2012; Brinkmann, Weinzierl, 2018; Ben-Hur *et al.*, 2019). Here, the question is inverted – what is the appropriate maximum order of SH given a certain sampling scheme?

In theory, the least-squares solver can deal with any number of basis functions. If the number of functions is lower than the number of sampling points (an overdetermined system), the solver will try to minimize the error between the original data and the approximation. Otherwise, the values at the sampling points will be preserved and the data between them will be interpolated. The latter case, however, is prone to overfitting, and thus an overdetermined system is a more reliable choice, even though it does not keep the original data intact.

With SH often referred to as a 2D equivalent of Fourier series, some analogy for equiangular grids can be made regarding Nyquist's sampling theorem. As an example, a grid of 15° angular resolution results in 360°/15° = 24 points around the sphere in either the horizontal or vertical plane. To avoid the aliasing phenomenon, the maximum spatial frequency should be less than half of that, i.e., no more than 11 cycles per full rotation. The spatial frequency over the azimuthal and inclination angles corresponds directly to the SH order and degree, respectively, so in the case of 15° resolution, the maximum allowed order should be 11. Likewise, for 10° resolution, the maximum order can be no greater than 17. The same maximum order limits of 11 and 17 were adopted for the equiareal grids consisting of 266 and 614 points, respectively.

4.2. Alternative interpolation methods

Interpolation on the sphere can be handled as the 2D interpolation of a periodic function $f(\phi, \theta)$. The choice of algorithms acting as references for the spherical harmonics approximation (SHA) was based on solutions known from HRTF interpolation, which has been more widely investigated than sound source directivity interpolation.

The most basic interpolation method is the nearest neighbor (NN) approach, whereby values for all the desired points are simply copied from the closest points on the original grid. No extra calculations are needed beside rounding to the nearest data point, which is why NN is sometimes referred to as naive and can serve as a basic reference method. NN can be applied to both regular and irregular grids; how the nearest point is determined will change, but the core idea remains the same.

Data from a regular grid have the same properties as a digital image, and there are thus plenty of interpolation algorithms, with bilinear, bicubic, and spline methods being the most popular. One-dimensional versions of linear and spline interpolation have been successfully applied in the median plane of HRTFs (Nishino *et al.*, 1999), and thus their 2D extensions were chosen for comparison with the proposed method.

Interpolation algorithms for irregular grids are more complex, as they require more universal definitions. Referring to HRTFs once again, the problem of choosing an appropriate interpolation algorithm was tackled in a recently developed robust spatial sound library, 3D Tune-In Toolkit (Cuevas-Rodriguez *et al.*, 2019). The authors of this toolkit acknowledged the advantages of SHA, but they were discouraged by potential problems when using custom grids (the library allows for importing bespoke sets of HRTFs). Instead, they decided to use an algorithm based on barycentric weights, which is a simplification of an interpolation method introduced by Gamper for distance-dependent HRTFs (Gamper, 2013). The algorithm constructs a triangle around the interpolated point using the three nearest points, and then calculates a value based on the data at the triangle vertices, taking into account the distance from each vertex to the interpolated point. The algorithm can be used for any point distribution[4], but is potentially less effective than SHA Cuevas-Rodriguez *et al.*, 2019).

[4]For some of the interpolated points lying on the equator, the three nearest points all lied on the equator as well and therefore no triangle could be formed. For these points, interpolation was performed only basing on the two nearest points and the algorithm was scaled one dimension down.

4.3. Measure of error

As measurement data are only available in certain discrete directions, the approximation or interpolation error can only be determined in a limited number of directions. The contribution of these points to the mean error has to be considered in a similar way as for the approach to obtaining the coefficients F_{lm} (see Subsec. 4.1.1). The mean error measure is based on the area-weighted spatial standard deviation introduced by Leishman to describe the omnidirectionality of a sound source for a given frequency band in the form of a single value (Leishman *et al.*, 2006). The standard deviation is replaced by the root-mean-square error to give the area-weighted root-mean-square error (AWRMSE):

$$\mathrm{AWRMSE} = \sqrt{\frac{\sum_{k=1}^{K} w_k \left(f_a(\Omega_k) - f_r(\Omega_k)\right)^2}{\sum_{k=1}^{K} w_k}}, \qquad (11)$$

where $f_a(\Omega_k)$ are computed values (obtained by approximation or interpolation on sparse measurement results), $f_r(\Omega_k)$ are reference values (obtained by measurements on a finer grid), and w_k are the weights defined in Eqs (9) and (10). Both $f_a(\Omega_k)$ and $f_r(\Omega_k)$ are given in decibels.

5. Accuracy of the directivity retrieval

5.1. Maximum-order-based analysis

Spherical harmonic approximation was applied to each of eight sparse datasets (2 sound sources × 2 sampling densities × 2 grid types) to obtain values on the 5° equiangular grid. Computations were carried out for each 1/3 octave frequency band in the range of 1–16 kHz and each possible maximum order of SH ranging from 3 to 11 or 17, depending on the sparse grid resolution. Figure 5 shows the results for all the experimental setups.

In general, as expected, a higher maximum order of SH produces a lower error. Sometimes, minor overfitting occurs, but only for the highest maximum orders of SH. AWRMSE varies significantly depending on the original directivity patterns, which vary for different sound sources (compare Figs 5a and 5b). The patterns also change with frequency, tending to take increasingly complex shapes with each consecutive frequency band, which results in higher error values.

The plots that differ only in the grid type (Figs 5a and 5c) have similar shapes, yet for the equiareal grid, all the AWRMSE values are higher. For lower maximum orders of SH, using more densely sampled data only improves the accuracy slightly (compare Figs 5b and 5f). The higher resolution, however, allows for efficient use of higher-order SH. In contrast, exceeding the imposed maximum order limit results in large numerical errors for regular grids and overfitting for irregular ones.

5.2. Comparison with alternative methods

The alternative interpolation algorithms described in Subsec. 4.2 were applied to each of the datasets, and the AWRMSE values for each dataset were calculated. To present the results conveniently, the AWRMSE values were averaged over all the analyzed frequency bands, and these mean values (denoted as AWRMSE_μ) were subjected to further analysis. In this section, AWRMSE_μ is a single value that represents the average error of the data on the 5° – resolution equiangular grid obtained from a given sparse grid, for a given sound source, and using a given method. The results for both loudspeakers are presented in Fig. 6.

When using the averaged AWRMSE values, the general trend of decreasing the error as the maximum order of SH increases is even more prominent. However, even when using the highest maximum orders, the alternative interpolation methods still provide better accuracy, except for the NN algorithm. As the simplest solution to any interpolation problem, NN was considered as a benchmark in the comparison, and SHA outperforms it even for lower maximum orders (starting from 4–8, depending on the dataset).

When precision is the highest priority, the best interpolation algorithms are the barycentric method (for equiareal grids) and the linear or spline approach (for equiangular grids). The difference in accuracy between these methods and SHA is small. Excluding the results for NN, the absolute AWRMSE_μ values for all methods are below 1 dB for the sparser grids and below 0.5 dB for the denser ones. Considering that 1 dB is widely acknowledged as the just-noticeable difference in human sound level perception (Fastl, Zwicker, 2006), this seems like a reasonable trade-off for reducing the number of measurement points by almost 89% (sparser grids) and 76% (denser grids)[5].

Even though SHA resulted in slightly higher mean retrieval errors, it does not mean that this method is necessarily worse than the alternatives. Using basis functions has several advantages, with the clearest being the infinite resolution without the need for additional computation; once the coefficients for SH have been determined, data for any direction can be easily obtained. Additionally, the benefits of expressing the sound source directivity in the SH domain have been proven by numerous studies using this technique, some of which have been cited in this paper.

[5]This trade-off should not be applied for commercial purposes. Authors do not intend to encourage anybody to publicly share interpolated directivity data in formats such as GLL or CLF, which are meant to represent true measurement data.

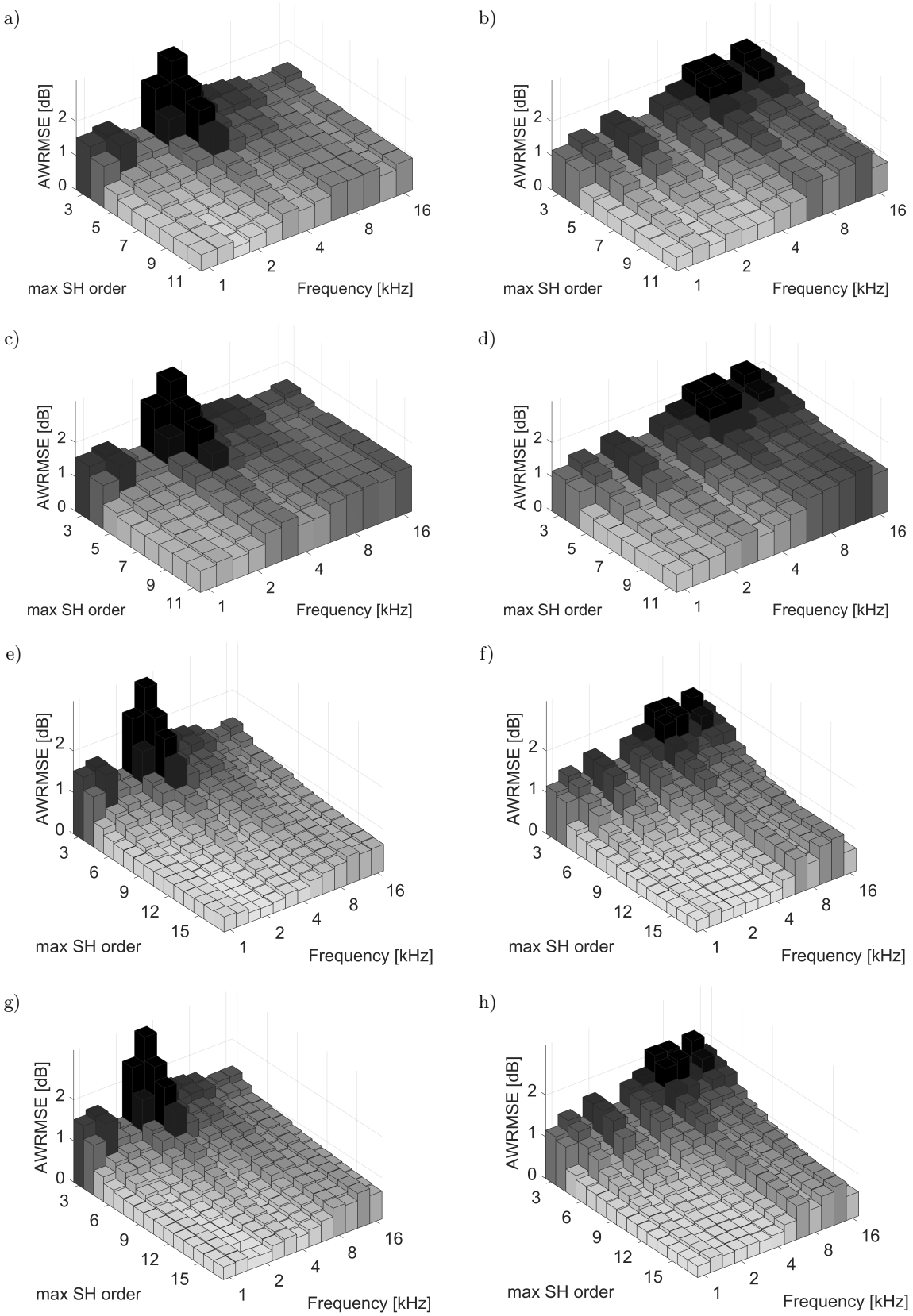

Fig. 5. Bar plots of AWRMSE values for SHA depending on maximum SH order and frequency band for different setups: a) loudspeaker system A, 15° equiangular grid, b) loudspeaker system B, 15° equiangular grid, c) loudspeaker system A, 266-points equiareal grid, d) loudspeaker system B, 266-points equiareal grid, e) loudspeaker system A, 10° equiangular grid, f) loudspeaker system B, 10° equiangular grid, g) loudspeaker system A, 614-points equiareal grid, h) loudspeaker system B, 614-points equiareal grid.

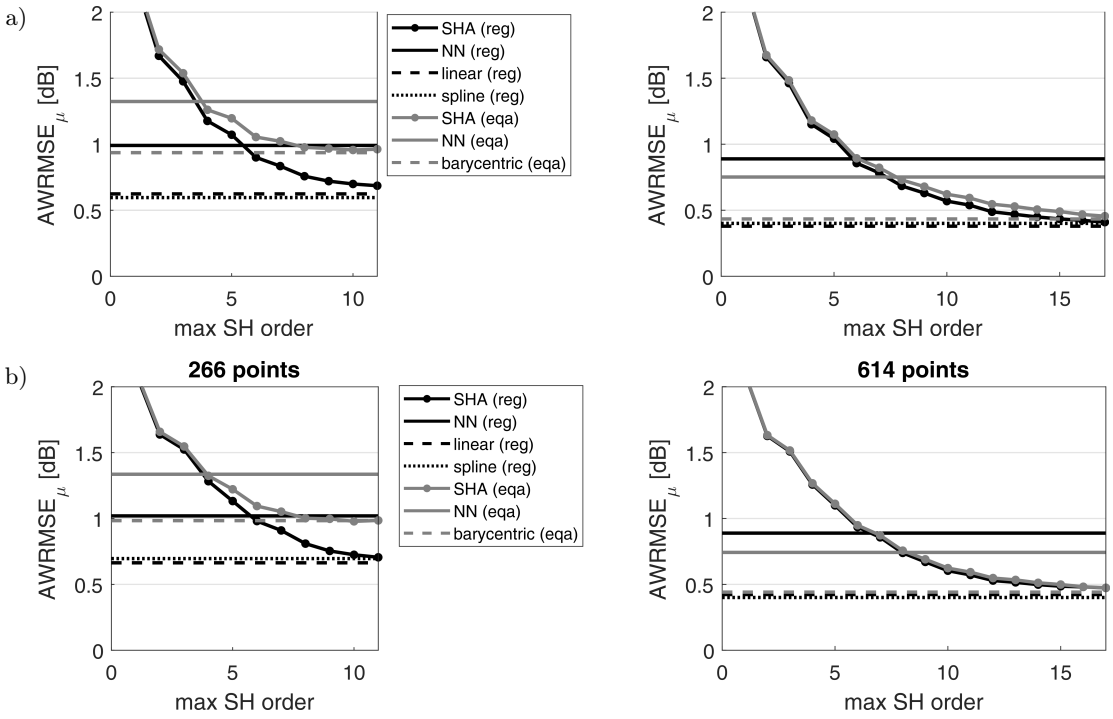

Fig. 6. Comparison of SHA with alternative interpolation methods at both analyzed resolutions: sparser on the left and denser on the right. Black lines (denoted in the legend as "reg") denote results obtained from regular equiangular grids (15° resolution on the left and 10° on the right), whereas gray lines (denoted as "eqa"") denote results obtained from equiareal grids with the same number of points as the corresponding equiangular grids (266 and 614, respectively): a) loudspeaker system A, b) loudspeaker system B.

The interpolation of data from the 266-points equiareal grid yielded much larger errors than interpolation from the other datasets. This discrepancy was also apparent when using the alternative methods (NN for the regular grids performed much worse than NN for the equiareal grids, the barycentric method performed much worse than the linear or spline approach). This effect occurred for both loudspeaker systems, but only for the sparser of the equiareal measurements. As the grids for both 266 and 614 points were designed in the same way, it can be assumed that the data were measured and processed correctly. Such results might occur when some of the determined 266 points do not efficiently represent their respective zones, despite using the correct algorithm. What makes this explanation even more probable is that the discrepancy in the AWRMSE$_\mu$ values is much lower for low maximum SH orders: in this case, the potential presence of outliers would have less of an impact on the results, as the low-order SH allow for retrieval of only a general shape of the directivity pattern. This issue emphasizes the importance of an appropriate choice of sampling points.

With the exception of the NN algorithm for the denser grids, the equiangular approach generally leads to smaller errors than the equiareal one. This is particularly interesting for SHA, where not only was the algorithm expected to benefit from a more equal distribution of sampling points, but also regular grids require more advanced computations using weighted least-squares. Additionally, the applied weights were not exact, but approximated (see Subsec. 4.1.1).

6. Cross-scheme evaluation

To examine more closely the effects of the sampling scheme choice on the accuracy of the retrieved results, a cross-scheme evaluation was performed. All possible pairs were formed from the available sparse datasets and the data were resampled by means of SHA. The procedure was exactly the same as described in the previous section, save for the reference function and corresponding weights in Eq. (11). The mean AWRMSE values (AWRMSE$_\mu$) for these resampled data are presented in Table 1.

The main finding of the comparison is that for every pair of grids the resampling error is lower when going from an equiareal grid to an equiangular one than the other way around. This might suggest that the SH representations obtained using the equiareal sampling schemes are closer to the actual directivity functions than the equivalents using the equiangular schemes. This idea might seem to contradict the conclusions from the previous section, but it is important to bear in mind that those computations were focused on obtaining the best accuracy on the 5° equiangular

Table 1. Cross-scheme evaluation results in the form of $AWRMSE_\mu$ [dB]. X → Y indicates that data measured on grid X were resampled by means of SHA to obtain values on grid Y, and *vice versa*; 15° and 10° denote the equiangular grid resolution; 266 and 614 denote the number of points in the equiareal grids.

X	Y	Loudspeaker system A		Loudspeaker system B	
		X → Y	Y → X	X → Y	Y → X
15°	266	1.03	0.92	1.09	0.98
10°	614	0.62	0.61	0.62	0.61
15°	614	0.72	0.59	0.71	0.58
10°	266	0.99	0.96	1.02	1.00
15°	10°	0.66	0.54	0.70	0.57
266	614	0.93	0.96	0.96	0.99

grid, not necessarily the best continuous representation.

There is a significant difference between the results for pairs going to or from the 266-point equiareal grid and the results for the remaining pairs. The potential reason for this was discussed in Subsec. 5.2. However, the subject of the error magnitude depending on the direction remains open and will be considered in future research.

7. Conclusions

The results presented in this paper show that spherical harmonics (SH) can be successfully used to increase the resolution of a sparsely measured sound source directivity. When using a proper number of basis functions (choosing the right maximum order of SH), data with a 5° resolution can be retrieved with a mean error of less than 1 dB for a 15°-resolution measurement, and less than 0.5 dB for a 10°-resolution measurement. The results are significantly better than those achieved by the naive nearest neighbor interpolation, and are comparable with those obtained by means of more advanced 2D interpolation algorithms such as spline methods or an algorithm based on barycentric coordinates. At the same time, spherical harmonic approximation offers some other benefits over these more advanced methods, such as the infinite resolution of the results or reduced amount of memory required to store the data.

The accuracy of the directivity retrieval depends heavily on the distribution of the sampling points. A comparison of the resampling errors between various grids using SH leads to the conclusion that there is no single best sampling scheme; if the goal is to obtain data on the standard 5°-resolution equiangular grid, interpolation from another, sparser equiangular grid will yield better results than interpolation from a grid with the same number of points that are distributed more evenly in terms of the distance between adjacent points. However, if the goal is to obtain the best continuous representation of the directivity, the latter approach will be more efficient.

Acknowledgments

The authors would like to thank Klara Juros and Daniel Kaczor for their help in performing the measurements and their input in the early stages of the research.

References

1. CLF Group (2004), A common loudspeaker file format, *SynAudCon Newsletter*, **32**(4): 14–17.

2. AES56-2008 (2008), *AES standard on acoustics – Sound source modeling – Loudspeaker polar radiation measurements.*

3. Ben-Hur Z., Alon D.L., Rafaely B., Mehra R. (2019), Loudness stability of binaural sound with spherical harmonic representation of sparse head-related transfer functions, *EURASIP Journal on Audio and Music Processing*, **2019**(1): 5, doi: 10.1186/s13636-019-0148-x.

4. Brinkmann F., Weinzierl S. (2018), Comparison of head-related transfer functions pre-processing techniques for spherical harmonics decomposition, [in:] *Proceedings of the AES International Conference on Audio for Virtual and Augmented Reality*, Paper P9-3, http://www.aes.org/e-lib/browse.cfm?elib=19683.

5. Cuevas-Rodriguez M. *et al.* (2019), 3D tune-in toolkit: An open-source library for real-time binaural spatialisation, *PLoS ONE*, **14**(3): e0211899, doi: 10.1371/journal.pone.0211899.

6. Duan W., Kirby R. (2012), A hybrid finite element approach to modeling sound radiation from circular and rectangular ducts, *The Journal of the Acoustical Society of America*, **131**(5): 3638–3649, doi: 10.1121/1.3699196.

7. Evans M.J., Angus J.A.S., Tew A.I. (1998), Analyzing head-related transfer function measurements using surface spherical harmonics, *The Journal of the Acoustical Society of America*, **104**(4): 2400–2411, doi: 10.1121/1.423749.

8. Fastl H., Zwicker E. (2006), *Psychoacoustics: Facts and Models*, Springer-Verlag.

9. Felis J., Flach A., Kamisiński T. (2012), Testing of a device for positioning measuring microphones in anechoic and reverberation chambers, *Archives of Acoustics*, **37**(2): 245–250, doi: 10.2478/v10168-012-0032-5.

10. Gamper H. (2013), Head-related transfer function interpolation in azimuth, elevation, and distance *The Journal of the Acoustical Society of America*, **134**(6): EL547–EL553, doi: 10.1121/1.4828983.

11. Hargreaves J.A., Rendell L.R., Lam Y.W. (2019), A framework for auralization of boundary element method simulations including source and receiver directivity. *The Journal of the Acoustical Society of America*, **145**(4): 2625–2637, doi: 10.1121/1.5096171.

12. Joseph P., Nelson P.A., Fisher M.J. (1999), Active control of fan tones radiated from turbofan engines. I. External error sensors, *The Journal of the Acoustical Society of America*, **106**(2): 766–778, doi: 10.1121/1.427095.

13. Leishman T.W., Rollins S., Smith H.M. (2006), An experimental evaluation of regular polyhedron loudspeakers as omnidirectional sources of sound, *The Journal of the Acoustical Society of America*, **120**(3): 1411–1422, doi: 10.1121/1.2221552.

14. Leopardi P. (2005), Recursive zonal equal area sphere partitioning toolbox, *Matlab Software Package Available via SourceForge*, http://eqsp. sourceforge. net.

15. Leopardi P. (2006), A partition of the unit sphere into regions of equal area and small diameter, *Electronic Transactions on Numerical Analysis*, **25**: 309–327.

16. Lidoine S., Batard H., Troyes S., Delnevo A., Roger M. (2001), Acoustic radiation modelling of aeroengine intake comparison between analytical and numerical methods, [in:] *7th AIAA/CEAS Aeroacoustics Conference and Exhibit*, doi: 10.2514/6.2001-2140.

17. Mobley F. (2015), Interpolation of aircraft source noise directivity patterns modeled by spherical harmonics, [in:] *Proceedings of Meetings on Acoustics*, Vol. 25, doi: 10.1121/2.0000193.

18. Nishino T., Kajita S., Takeda K., Itakura F. (1999), Interpolating head related transfer functions in the median plane, [in:] *IEEE ASSP Workshop on Applications of Signal Processing to Audio and Acoustics*, pp. 167–170, IEEE, doi: 10.1109/aspaa.1999.810876.

19. Pasqual A.M. (2014), Spherical harmonic analysis of the sound radiation from omnidirectional loudspeaker arrays, *Journal of Sound and Vibration*, **333**(20): 4930–4941, doi: 10.1016/j.jsv.2014.05.006.

20. Politis A. (2016), *Microphone array processing for parametric spatial audio techniques*, Doctoral dissertation, Aalto University.

21. Rayleigh J. (1945), *The Theory of Sound*, Number 1 in The Theory of Sound, 2nd ed., Macmillan.

22. Shabta N.R., Behler G., Vorländer M., Weinzierl S. (2017), Generation and analysis of an acoustic radiation pattern database for forty-one musical instruments, *The Journal of the Acoustical Society of America*, **141**(2): 1246–1256, doi: 10.1121/1.4976071.

23. Sinayoko S., Joseph P., McAlpine A. (2010), Multimode radiation from an unflanged, semi-infinite circular duct with uniform flow, *The Journal of the Acoustical Society of America*, **127**(4): 2159–2168, doi: 10.1121/1.3327814.

24. Snakowska A., Jurkiewicz J. (2010), Efficiency of energy radiation from an unflanged cylindrical duct in case of multimode excitation, *Acta Acustica united with Acustica*, **96**(3): 416–424, doi: 10.3813/AAA.918294.

25. Snakowska A., Jurkiewicz J., Gorazd Ł. (2017), A hybrid method for determination of the acoustic impedance of an unflanged cylindrical duct for multimode wave, *Journal of Sound and Vibration*, **396**: 325–339, doi: 10.1016/j.jsv.2017.02.040.

26. Sneeuw N. (1994), Global spherical harmonic analysis by least-squares and numerical quadrature methods in historical perspective, *Geophysical Journal International*, **118**(3): 707–716, doi: 10.1111/j.1365-246X.1994.tb03995.x.

27. Zhang W., Abhayapala T.D., Kennedy R.A., Duraiswami R. (2010), Insights into head-related transfer function: Spatial dimensionality and continuous representation, *The Journal of the Acoustical Society of America*, **127**(4): 2347–2357, doi: 10.1121/1.3336399.

28. Zhang W., Zhang M., Kennedy R.A., Abhayapala T.D. (2012), On high-resolution head-related transfer function measurements: An efficient sampling scheme, *IEEE/ACM Transactions on Audio, Speech and Language Processing*, **20**(2): 575–584, doi: 10.1109/TASL.2011.2162404.